



## Applying FDEM, ERT and GPR at a site with soil contamination: A case study



Tzu-Pin Wang<sup>a,b,\*</sup>, Chien-Chih Chen<sup>a</sup>, Lun-Tao Tong<sup>c</sup>, Ping-Yu Chang<sup>a</sup>, Yi-Chieh Chen<sup>d</sup>, Tien-Hsing Dong<sup>e</sup>, Hsin-Chang Liu<sup>f</sup>, Chih-Ping Lin<sup>f</sup>, Kai-Hsing Yang<sup>g</sup>, Ching-Jen Ho<sup>g</sup>, Shih-Nan Cheng<sup>b</sup>

<sup>a</sup> Dep. of Earth Sciences and Graduate Institute of Geophysics, National Central University, Taiwan

<sup>b</sup> Disaster Reduction Research Center, Chien Hsin University of Science and Technology, Taiwan

<sup>c</sup> Industrial Technology Research Institute, Taiwan

<sup>d</sup> Geophysical Technology and Engineering Co., Ltd., Taiwan

<sup>e</sup> Apollo Technology Co., Ltd., Taiwan

<sup>f</sup> D.P.W.E. National Chiao Tung University, Taiwan

<sup>g</sup> Environmental Protection Administration, Taiwan

### ARTICLE INFO

#### Article history:

Received 4 December 2014

Received in revised form 1 July 2015

Accepted 6 July 2015

Available online 16 July 2015

#### Keywords:

GPR

ERT

EM

Soil pollution

Remediation evaluation

### ABSTRACT

This study employed the combination of three methods, namely the Frequency Domain Electromagnetic (FDEM), Electrical Resistivity Tomography (ERT) and Ground Penetrating Radar (GPR) to evaluate a heavy-metal contaminated site for both pre- and post-remediation investigations. The main goals were to verify the position and the integrity of the underground storage tanks (UST), and to determine the effectiveness of remediation to ensure no contaminants remained at the site. In general, the GPR survey was effective at locating shallowly buried objects. However, due to the highly conductive nature of the heavy-metal laden sludge, the GPR signals were attenuated severely. Thus, the first attempt to use GPR in the pre-remediation investigation did not achieve the desired results and other methods were deployed. The existence of the UST and the sludge within were confirmed by ERT and the UST shape was mapped by FDEM. The principal remediation scheme was soil replacement by replacing the contaminated soil with clean silt. Based on the distinctive property differences of the contaminated soil and the clean silt, the completion of the remediation was confirmed by the differences between pre-remediation and post-remediation in GPR, ERT and FDEM results.

© 2015 Elsevier B.V. All rights reserved.

### 1. Introduction

With the enhancement of environmental awareness, Taiwan holds an increasingly positive attitude for facing soil and groundwater pollution problems. Taiwan Environmental Protection Administration (TEPA) has the power to require polluters to remediate contaminated sites. Otherwise, TEPA can suspend the operation of a plant or debar the transfer of the land's ownership. Therefore, many private sectors have actively taken initiatives to conduct contamination investigations and remediation work. Over the past five years, TEPA has obtained many good results in soil and groundwater pollution investigations by employing geophysical prospecting techniques. For example, TEPA used Ground Penetrating Radar (GPR) to reveal buried pipelines that a plating factory illegally discharging sewage with, Electrical Resistivity Tomography (ERT) to discover a Non-aqueous phase liquid (NAPL) pool and Frequency Domain Electromagnetic (FDEM) to define the actual coverage of a landfill.

These three techniques are also listed as being recommended for contamination investigation by TEPA. In addition to using these methods in pre-remediation investigations, TEPA also expects to promote the application of geophysical methods alongside traditional sampling and analysis in post-remediation investigations to assess the effectiveness of remediation work.

GPR, ERT and FDEM are able to efficiently define the electrical properties of shallow layers. With applications of geology, geochemistry, microbiology and sampling and analysis, they are often employed in soil and groundwater contamination investigations (Atekwana and Atekwana, 2010). GPR has proven its ability to provide high-resolution images for strata. Thus, it is useful for investigations in geology, archeology and buried structures and pipelines (Al-Nuaimy et al., 2000; Beauprêtre et al., 2012; Porsani et al., 2010; Tohge et al., 1998). In environmental pollution investigations, GPR can survey the NAPL leakage distribution (Cassidy, 2007; Greenhouse et al., 1993; Lopes de Castro and Branco, 2003). Annan (2002) provides a comprehensive review of the development history and applications of GPR. ERT was mainly used in geological research in its early stage. The applications of ERT have since extended to environmental pollution investigations. For example, ERT can survey pipeline or tank leak incidents, verify sewage

\* Corresponding author at: Dep. of Earth Sciences and Graduate Institute of Geophysics, National Central University, Taiwan.

E-mail addresses: [wtbin@uch.edu.tw](mailto:wtbin@uch.edu.tw) (T.-P. Wang), [chenc1972@gmail.com](mailto:chenc1972@gmail.com) (C.-C. Chen).

leakage and define the scope and depth of landfills (Ayolabi et al., 2013; Batayneh, 2005; Dahlin et al., 2002; Godio and Naldi, 2003; Marti'nez-Paga'n et al., 2010). During or post-remediation work, ERT can assess or confirm remediation results or indicate locations that require further improvement (Goes and Meeke, 2004; Halihan et al., 2005). Electromagnetic methods are often used in metal mineral surveys. In 1980s, the one-man portable terrain conductivity meters (FDEM) were

developed to map the apparent conductivity in the shallow surface and provide contour images. By examining the contour images, stratum structures or buried objects can be studied. Due to its quick and easy operation, FDEM has shown its usefulness in massive area investigations, such as in archeological studies (Batmunkh et al., 2004; Conyers et al., 2008) or in saline intrusion investigations (Holman and Hiscock, 1998). In addition, in the case of geological disasters, FDEM facilitates search and rescue

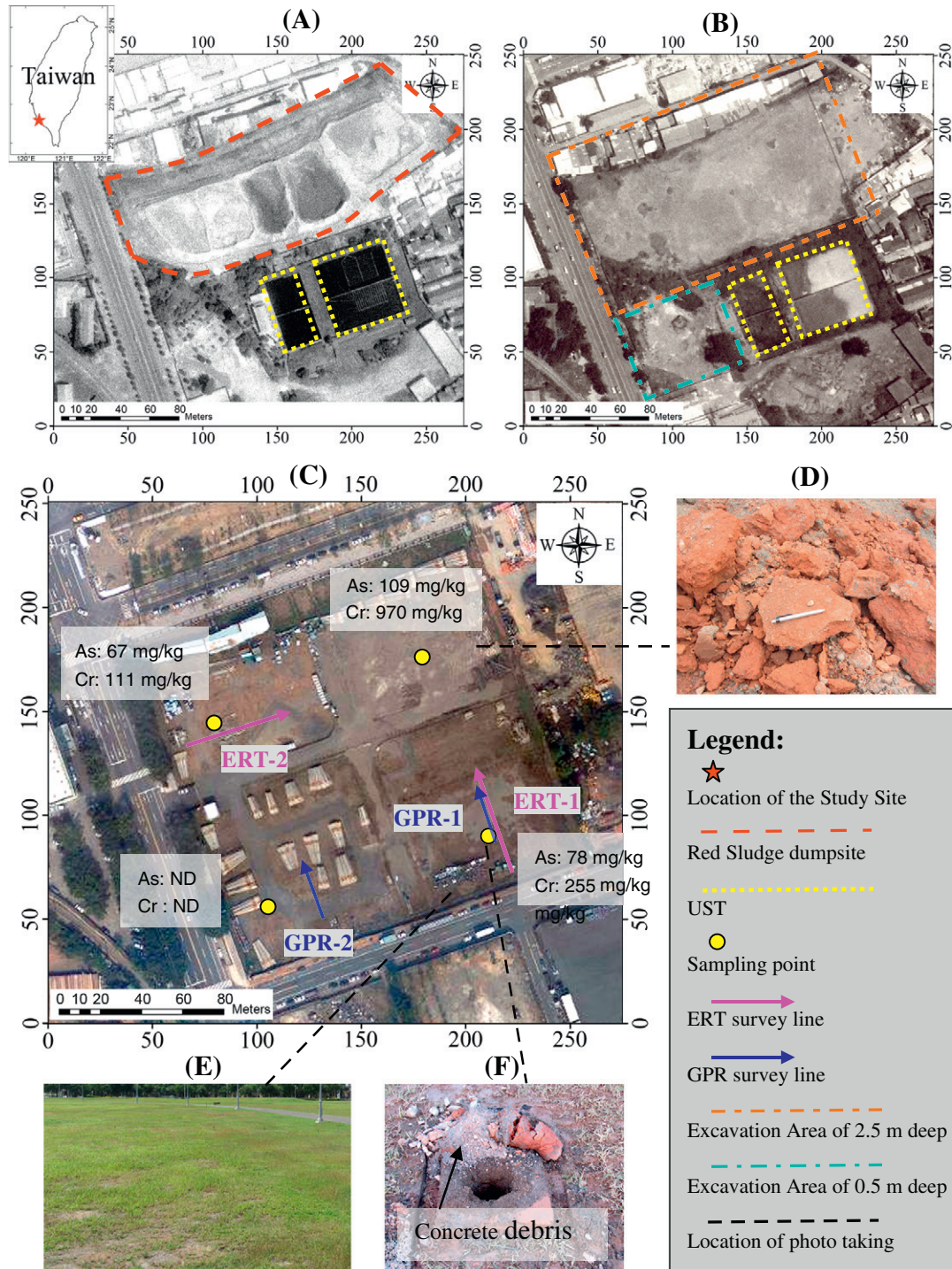


**Fig. 1.** Site description: (A) In 1980s, a waste disposal area was located in the north part of the study site; in the southeast, there were two sedimentation tanks of different sizes. All of the aerial photograph coordinates were redefined as X: 0–275; Y: 0–250 m. (B) In 1990s, the factory closed and the sludge stacking area in the north was leveled. The USTs were left in the southeast. (C) In 2000s, the site was converted into a green park. In 2010, soil sampling found Cr and As contamination at the site, except in the southwest. The remediation plan was to unearth at least 2.5 m of soil in the north and approximately 0.5 m of soil in the southwest; the remediation was based on the geophysical prospecting in the southeast. (D) Red sludge in the north. (E) Site photos (2012). (F) Photos of soil sampling at the UST locations (2012); the layer of red sludge was 0.312 m thick; the concrete material was located at a depth of 1.2 m. The sampling diameter was 6 cm.

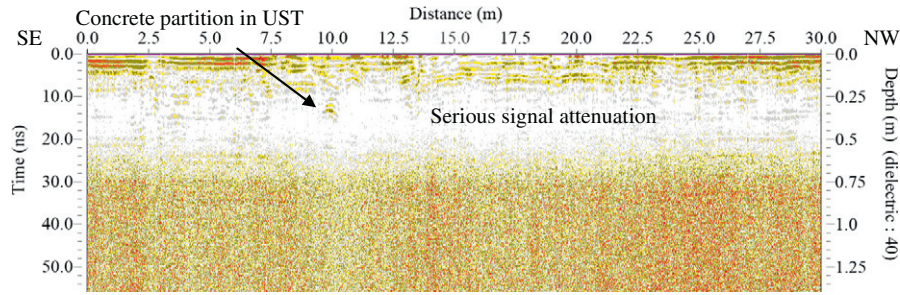


Fig. 2. Pre-remediation of the GPR-1 profile. When the dielectric was set to 40, such as for clay with high conductivity, it can be used as the depth reference.

operations and can locate vehicles or houses buried under debris to provide information for excavation and searching priorities (Yu et al., 2009). If there are NAPL leaks or landfill leachate, FDEM can also depict the distribution of the pollution (Nobes et al., 2000; Pettersson and Nobes, 2003).

Each method has its own distinct advantages, limitations, and dimensions in which it is appropriate to use. When one individual method survey cannot gather sufficient information to construct a holistic picture of the underground environment, multiple geophysical prospecting methods are combined. Integrating results of GPR, ERT, FDEM, magnetic and seismic refraction (SR) can help construct more accurate geological models (Bowling et al., 2007; Chang et al., 2012). GPR and ERT can gather sufficient detailed information about shallowly buried objects within small given areas (Ny'ari and Kanh, 2007; Pringle et al., 2012). Archeologists often use FDEM and magnetic methods to obtain a general idea about a massive subsurface range and use GPR and ERT to examine certain areas for depth (Batmunkh et al., 2004; Orlando, 2013; Tong et al., 2013). In environmental pollution studies, it is crucial to consider not only the physical properties of the pollutants but also the chemical reactions and microorganisms in the strata after the pollutant intrusion because the reactions will affect the survey results and mislead the interpretation for the underground settings (Atekwana et al., 2000). GPR, ERT and FDEM are the main methods that are often integrated in investigations of landfills, leachate and NAPL leakage to compensate one another in terms of their advantages and limitations. Each mode of combination endorses one another for each interpretation for the distribution of the contaminants both horizontally and vertically. The more comprehensive information an investigation can provide, the more successful the subsequent remediation and the contamination risk evaluation can be (Guérin et al., 2004; Hermozilha et al., 2010; Lago et al., 2009; Soupios et al., 2007; Vaudelet et al., 2011; Zogala et al., 2009).

This study is based on a case of a heavy-metal contaminated site in a southern Taiwan metropolitan area (Fig. 1). GPR, ERT and FDEM were used to verify the integrity of the underground storage tanks (USTs) and the existence of laden sludge. Due to the lack of records, it could only be inferred by the aerial photographs that USTs had once been

located at the site. Because the UST integrity and sludge distribution determined the funds and time for the remediation work, an urgent need for the remediation team was indicated. Being the most well-known geophysical prospecting method in Taiwan, GPR was specified in the remediation proposal to locate the UST even though not everyone understands what factors may impact GPR signals. In general, GPR is effective for investigating shallow-buried objects. However, the GPR signals were seriously attenuated when the pre-remediation investigation started and therefore, failed to collect operational data. Thus, other geophysical techniques were immediately adopted. When geophysical prospecting methods were subjoined, the remediation had begun and was ongoing. The remediation team desired information about the UST integrity as soon as possible to adjust the subsequent remediation methods and control the remediation schedule. In short, the geophysicists were not given much time and space to perform the investigation. The study site was in an urban area where many environmental interferences could affect the investigation. With the limited time and space, and considering the urban environmental interferences and the signal attenuation caused by the sludge, ERT and FDEM were adopted for their feasibility, mobility and lower sensitivity to environmental interferences. The geophysicists excluded SR and other EM methods due to the abovementioned inherited restrictions of temporal, special and environmental settings. The main pre-remediation investigation goals were to quickly verify the integrity of UST. The accuracy of the geophysical pre-remediation investigation was confirmed by excavation and sampling. This case study discussed the possible challenges to apply GPR, ERT and FDEM at sites where the environmental conditions are similar to the study site. The key implication was that by applying the same three methods in the pre- and post-remediation investigations, the geophysical methods cannot only efficiently obtain the information about the contaminated site in the pre-remediation investigation but can also be cost-effectively used to evaluate the accomplishment of the remediation in the post-remediation. Furthermore, in light of the discussion in this case study, the application of geophysical prospecting technology in a contaminated site investigation can be promoted.

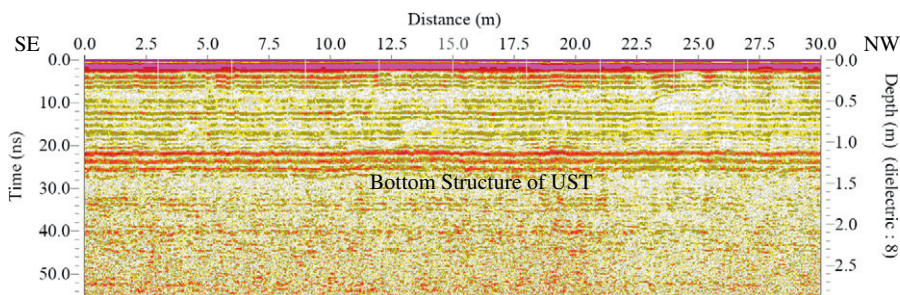
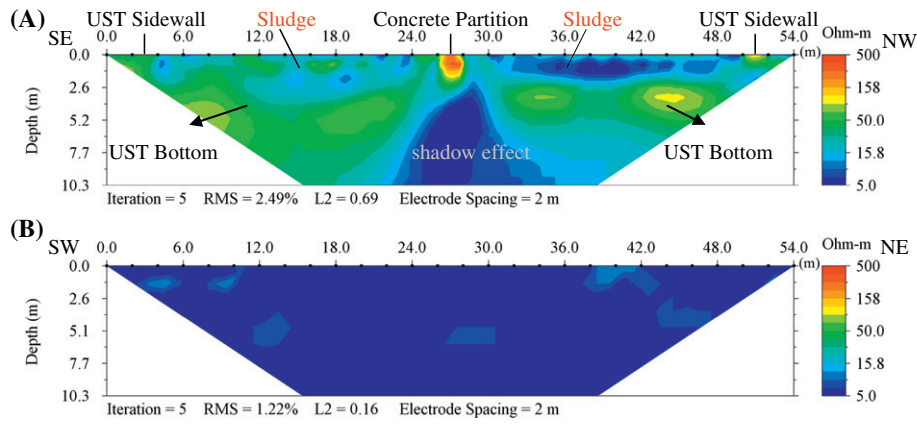


Fig. 3. Post-remediation GPR-1 profile.



**Fig. 4.** Pre-remediation ERT Profile. Resistivity coordinates on a log scale. (A) ERT-1 result. USTs should still be at the site with sludge inside. (B) ERT-2 result. No clear boundary is observed as the resistivity of the sludge is as low as that of the background stratum.

## 2. Site overview

This site was located on an alluvial plain classified as Holocene alluvium containing clay, silt and sand. Approximately 600 m from the coastline, the alluvial layer was more than 100 m thick with a clay-based surface. Therefore, the resistivity of the surface should be low. The land was approximately 30,000 m<sup>2</sup> wide and mainly used for an industrial waste dumpsite by an aluminum factory in 1960s. The industrial waste was red mud residue produced in the final stage of the aluminum refining process. During that time, the entire north part of the site was used to accumulate the red sludge. The main components of the sludge were Fe<sub>2</sub>O<sub>3</sub> and Al<sub>2</sub>O<sub>3</sub> containing heavy metals, such as lead, mercury, arsenic, and chromium. That is why the site was considered to be heavy-metal contaminated. The groundwater table was approximately 3.6 to 4 m deep, with large-scale flow from the northeast to the southwest. The groundwater sample presented no contamination. Thus, this site was only contaminated in soil. There were two different sizes of reinforced concrete USTs in the southeast portion of the study area. Each UST was divided into two parts by a thin concrete wall in the center (Fig. 1A). In 1990s, the factory was closed; however, the USTs were not removed and still contained the waste product (red sludge) (Fig. 1B). In 2000, the entire site was renovated as a green park (Fig. 1C). The red sludge and the USTs were completely invisible in the site photographs taken after 2010 (Fig. 1D and E).

In 2010, TEPA found the presence of heavy metals, including lead, mercury, arsenic, and chromium, in the soil samples of this site. The concentration of arsenic was 109 mg/kg and chromium was 970 mg/kg, which both exceed Taiwanese regulatory soil standards (i.e., As:

60 mg/kg, Cr: 250 mg/kg) (the locations for the soil sampling and analysis results are shown in Fig. 1C). Therefore, TEPA ordered the assessment of the amount of sludge, soil remediation and pollutant removal. The proposed solution was to unearth all the red sludge and backfill with clean silt. Based on the aerial photographs and the soil samples, the red sludge was throughout the north side. Drilling indicated that the depth of the sludge was approximately 2.5 m. Therefore, a large-scale excavation and dirt removal were expected, and to totally unearth the contaminated soil, the excavation depth must be greater than 2.5 m until the original clay sediment was reached. The southwest side was neither part of the manufacturing process zone nor the sludge stacking area. The samples taken from the southwest part did not present any significant contamination. To not leave any random contamination, the remediation team decided to remove the 0.5 m of the topsoil. Because there were no records for the UST removal, the uncertainty regarding the existence of the USTs was problematic. Manual sampling found red sludge with exceedingly high heavy-metal concentrations at 0.3–1.2 m in the stratum, suggesting where the USTs should be located, and at 1.2 m deep, a sheet of hard material hindered the manual sampling and concrete debris presented in the samples (Fig. 1F). Thus, the remediation team assumed that there was the UST bottom and supposed the presence of UST. However, the sampling was rather limited representative, and the information yielded was not sufficient to verify the UST integrity, whereas a geophysical prospecting survey can offer more comprehensive and in-depth information to facilitate the remediation and hence, collect sufficient information to confirm whether the USTs remained intact at the site. If the USTs were still intact with the sludge secured within them, the pollutants in the southeast should be

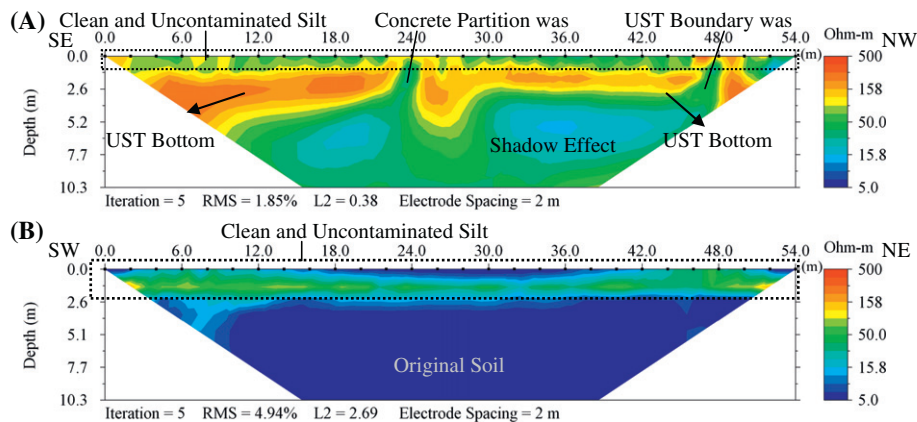


**Fig. 5.** Post-remediation ERT profile. Resistivity coordinates are on a log scale. (A) ERT-1 result. The result is still visible at the tank bottom, but the low resistivity indicates the sludge inside is gone. (B) ERT-2 result. Resistivity increased significantly after the removal of the shallow surface contaminated soil and by the replacement of the clean and dry silt.

retained inside the USTs without diffusion. Thus, large-scale excavation would be rebuffed in the southeast because it would damage the tank structure and release the sludge. Instead, small-scale excavation of the sludge within the tank would be performed, and the tank bottom would be left at the site after removing the contaminated soil. However, if the tanks were broken, the contaminated soil could have gone deeper than 1.2 m. If this was true, large instruments would be required to remove the tank structure and the depth of the contaminated soil would require re-assessment. Subsequently, the remediation cost and time would be significantly greater. In short, effective pre-remediation investigation is crucial.

### 3. Methodology

#### 3.1. GPR

GPR measures the electromagnetic wave reflection time (two-way time, TWT) after emitting high-frequency electromagnetic waves (1 MHz to 1000 MHz). By transmitting and receiving radio waves, GPR is used to probe the subsurface. The square root of the dielectric constant of the electromagnetic wave transmission speed and materials presents an inverse relationship; the electromagnetic wave transmission varies in phase and amplitude within different materials. Using the reflected electromagnetic signals expressed in plot images, the internal structure of the material can be analyzed (Annan et al., 1991; Annan and Davies, 1976; Davies and Annan, 1989). The GPR instrument in this study, the SIR-3000 system manufactured by Geophysical Survey Systems, Inc., had an antenna frequency of 400 MHz. To obtain high-quality informative data, the survey parameters were set to record one scanning datum for every 2.5 cm at a speed of approximately 1 m/s. Each scan curve was composed of 512 individual data points. Data processing used Radan software made by GSSI, and the data processing programs included Dewow, Deconvolution and Gain.

#### 3.2. ERT

ERT depicts the subsurface stratum structure images by the measured potential values. That is, ERT utilizes two electrodes, A and B, as current poles to inject the current into a stratum and two potential poles, M and N, to measure the potential difference in the stratum. Currently, automated multi-electrode instruments can quickly perform inversions on measured potential values, presenting them as true resistivity profiles. By the nature that different materials have different electrical properties, ERT images can describe the underground environment (Barker, 1981, 1991, 1992; Dahlin and Zhou, 2004; Griffiths and Turnbull, 1985; Griffiths et al., 1990; Griffiths and Barker, 1993; Loke, 1994; Loke et al., 2010a, 2010b, 2013; Zhou and Dahlin, 2003). The ERT instrument in this study was the SuperSting R8 system manufactured by Advanced Geosciences, Inc. Prior to formal testing, two types of high-resolution mixed electrode configurations, the Wenner–Schlumberger array and the dipole–gradient array, were tested at the site. The test parameters comprised an electrode spacing of 2 m, a maximal injection current of 500 mA, a measurement time of 3.6 s for each datum, 2 potential measurements for each datum, and the average of the 2 measurement results recorded as raw data. In addition, the error rate (%) for the two measurement results from each datum was calculated. The test results indicated that the error rate of the Wenner–Schlumberger array ranged between 0% and 1.1%. The average error rate for the data was 0.128%. The error rate for the data with the dipole–gradient array ranged between 0% and 6.9%. The average error rate for the data was 0.237%, indicating that the amount of data noise with the on-site measurement results of the dipole–gradient array was slightly greater than that in the results of the Wenner–Schlumberger array. Therefore, the Wenner–Schlumberger array was selected as the electrode combination. The resistivity data were inverted with the EarthImager2-D software. The software employs finite element forward solutions and an iterative conjugate gradient

inversion scheme, described in more detail by Yang (1999), to estimate the subsurface resistivity structure.

#### 3.3. FDEM

FDEM produces a primary electromagnetic field at 9.8 kHz, and this primary field induces a current in the strata; the induced current produces a secondary electromagnetic field, and on the other end, fixed to the instrument, is the receiver coil/loop that records the intensity of the secondary electromagnetic field to determine the conductivity of the materials in the stratum. By the phase shift/lag between the primary magnetic field and the secondary magnetic field, the conductivity of materials on the ground surface can be calculated. Mathematically, the secondary magnetic field signals can be divided into signals that are in phase with the same phase angle as the primary magnetic field and

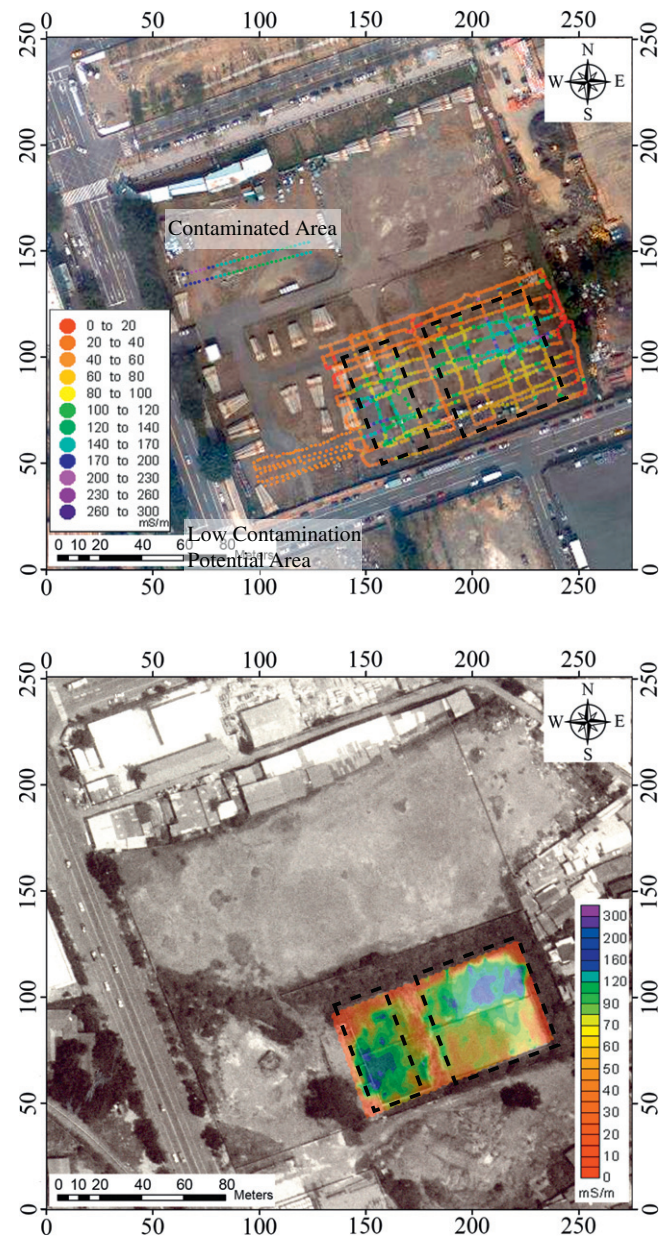


**Fig. 6.** Pre-remediation FDEM result. (A) Overlapping the raw data from the probe points with the aerial photographs from the 2000s. There are 60 data points in the sludge area in the north, 105 data points in the low-contaminated potential area in the southwest, and 3338 data points in the southeast. (B) Overlapping the contour maps and the aerial photographs from the 1990s. The pattern of high conductivity is identical to the shape of the UST structure.

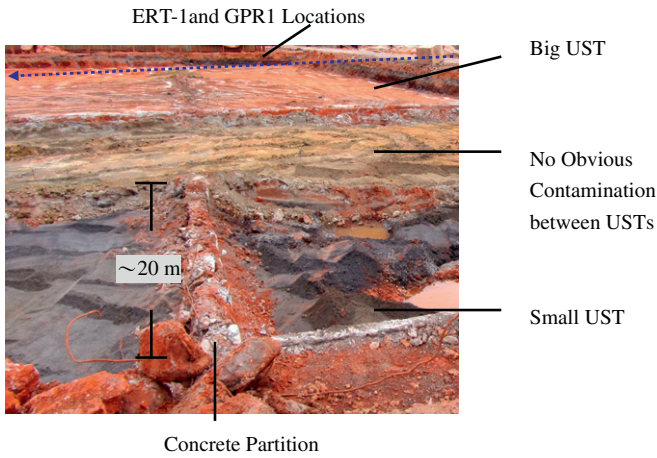


Fig. 7. Site photograph during UST remediation taken from (150, 70) towards the northeast.

signals that are out of phase (also called quadrature), which lag the primary field by  $90^\circ$ ; the amplitude of the two must be equal to the original wave. When the material conductivity increases, the phase-lag increases. In short, the in-phase component grows as the quadrature dwindles. Quadrature component is often converted into apparent conductivity, and when a series of conductivity data is plotted into a contour map, the characteristics of the material in the subsurface can be depicted (McNeill, 1980, 1990; Mussett and Khan, 2000; Nobe, 1999; Wightman et al., 2004). The FDEM instrument in this study was the CMD electromagnetic conductivity meter manufactured by GF Instruments, s.r.o. A 3-m-depth probe was used. The measurement method involved geophysicists carrying the instrument and walking on the site in a straight line while continually recording data. The walking speed was 0.8 m/s, and one data point including the apparent conductivity and in-phase signals, was recorded every second. The instrument was linked to a GPS device to confirm real-time recording of the absolute coordinates of each datum. The data processors were Sufer and ArcGIS of Golden Software, Inc., and Environmental Systems Research Institute, Inc., respectively.

## 4. Results

### 4.1. GPR

The sampling positions were used as control points for GPR-1 survey line. Based on the known-information that some suspected concrete was at the depth of approximately 1.2 m under the sampling points, there were two assumptions: one was that if strong signal reflections smoothly continued at the same depth, the USTs would be expected to be intact at the site; in contrast, if the reflections were intermittent as the depth varied or there were diffractions from suspected metal (steel), the bottom of the tank would be presumed to be damaged. However, the pre-remediation of the GPR-1 survey results, shown in Fig. 2, failed the two expectations. From 5 ns, the signals attenuated significantly, and at 8 ns, hardly any signal reflected. The only signal was a diffraction, which could be referred by the concrete partition inside of the UST, at 12 ns at a distance of 10 m, but the signal was not able to determine whether the UST bottom was intact. The high conductivity of the sludge was assumed to be responsible for the severe attenuation. Because the pre-remediation GPR results failed to realize their intended purpose, fine-tuning of the remediation plan and employment of other methods were necessary.

Subsequent investigations confirmed the existence and the integrity of the USTs. Accordingly, the UST area remediation was to unearth the sludge in the tanks and destroy the concrete partitions inside of the

USTs and the sidewalls thereof, but leave the tank bottoms where they were; then, backfill with clean and pollution-free soil taken from elsewhere. The post-remediation GPR-1 profile, shown in Fig. 3, displayed strong signal reflections continuing smoothly at 21 ns, where the tank bottoms remained, due to the clean silt replacement for the sludge. The post-remediation GPR profiles set the dielectric to 8 so that the setting could be used as the reference depth to meet the known-information that the tank bottoms were located at a depth of 1.2 m. In short, when the subsurface soil that severely attenuated the GPR signals was replaced, the GPR is capable of surveying shallowly buried objects.

### 4.2. ERT

After the GPR pre-remediation investigation, ERT was chosen hoping the resistivity profiles could define the UST integrity. The USTs were

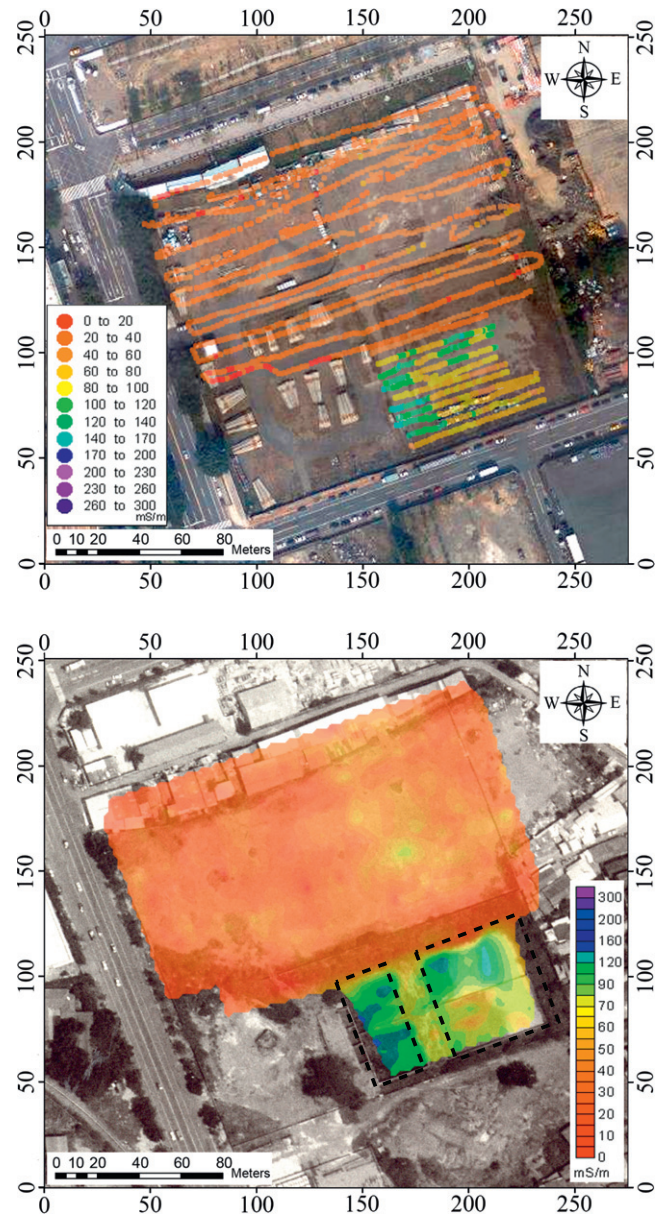


Fig. 8. Post-remediation FDEM result. (A) Overlapping map of survey points and the measured data and an aerial photograph taken in 2000s. Amount of Data Points: 7772 Points in the North (sludge dumpsite) and 2350 points in the Southeast (UST Area). (B) Overlapping the contour map and the aerial photograph from the 1990s. The dotted line shows the range of the original UST area.

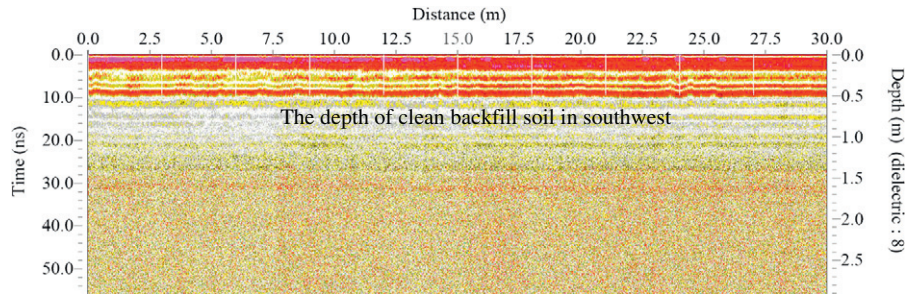


Fig. 9. Post-remediation GPR-2 profile.

composed of reinforced-concrete, including steel, but the steel was secured by the concrete so that the current could not penetrate. In other words, if the tank bottoms were intact, continuous high resistivity would be profiled. On the contrary, if the tank bottoms were gone or destroyed with the steel uncovered, the current would be able to conduct; therefore, the profiles would display inconsistent resistivity of high and low values. ERT-1 results, shown in Fig. 4A, displayed a continuous relative high resistivity in the strata (green color scale) where the tank bottoms were suspected to be located. At 27 m near the surface, there were high-resistivity anomalies that were indicative of the concrete partitions in the USTs. The cause of such profiles was believed to be the same as why the diffraction occurred at 10 m of GPR-1 survey line. High resistivity values were noted because of the wall-like concrete structure (partition) standing vertically in the ground and because the partition prevented the current from traveling between the electrodes. At 2 m and at 51 m, the same high resistivity profiles were presented and the two locations were presumed to be the UST boundaries. At the end of the survey line, with a limited amount of data, the high resistivity tomography was not as obvious as what the concrete partitions presented. Because the rest region near the surface showed low resistivity, it was presumed that the tanks were still filled with sludge. However, the depth defined by the low resistivity, which was sludge-suspected, differed from the analysis results obtained from the sampling points. The lower interface of the tank was somewhat deep. These results were because the ERT profiles were obtained after inversion, and inevitably, the resolution resulted with deviations, which hindered the depth of the tank bottoms depicting. In addition, objects buried underground are considered to be interferences for ERT. During measurement, the current cannot penetrate structures effectively, material reactions in the strata underneath the structures were difficult to depict. A shadow effect frequently appears during the inversion of this type of measurement data (Dahlin et al., 2002). Therefore, although ERT can interpret changes in phenomena and properties within strata, it cannot accurately depict the geometries of structures. Nevertheless, based on the response of continuous high resistivity values in ERT, it was determined that the tanks remained at the site.

ERT-2 investigation at the sludge dumpsite surveyed contaminated soil resistivity, results shown in Fig. 4B, and learned the thickness of the sludge was approximately 2.5 m deep according to sampling and analysis. However, the results showed low resistivity (<10 ohm-m)

throughout the strata, and no clear boundary of the sludge could be defined; therefore, the thickness of the sludge could not be concluded. In short, because the resistivity of the stratum constituents was similar to those of the contaminated soil material, no clear interface could be observed. Nevertheless, the ERT-2 profiles supported ERT-1 results that the low resistivity near the surface in Fig. 4B should be caused by the sludge.

Due to the changes in the site environment after the remediation work, the post-remediation ERT-1 survey line was shifted slightly to the northwest by 3 m, whereas the ERT-2 survey line was set in the same line as the pre-remediation investigation. Post-remediation ERT-1 profile showed that the resistivity of the materials at shallow surface increased significantly (Fig. 5A) due to the dry and clean silt replacement. However, a continuous pattern of high resistivity was still in the strata that indicated the tank bottom existence. Discontinued high resistivity signals at the distance of 24 m and at 48 m were presumed to be the inner partitions and the boundaries of the USTs. During the remediation process, the sidewalls and the partition of the USTs were destroyed, exposing the steel (see Fig. 7), and discontinuing the high resistivity pattern.

The low resistivity presented underneath the tank bottom was due to the structure of the tank bottom that remained intact at the site. The data gathered underneath the tank bottom showed a shadow effect generated by the inversion rather than the response of the geological materials. Post-remediation ERT-2 investigation showed the resistivity of shallow buried materials that increased significantly and depicted a clear excavation boundary (Fig. 5B). The low resistivity in the deeper strata, shown in Fig. 5B, was the same as that gathered from the pre-remediation survey. The low resistivity should be from the original geological materials with high conductivity. The interface of high and low resistivity presented itself at a depth of 2.5 m, which was also the excavation depth in the north. ERT post-remediation investigation indirectly verified the remediation results. Post-remediation soil sampling and analysis did not indicate the presence of heavy metals in soil.

#### 4.3. FDEM

If a more comprehensive investigation of structures buried underground had been performed using only ERT method, more survey lines, time, and human resources would be necessary to confirm the

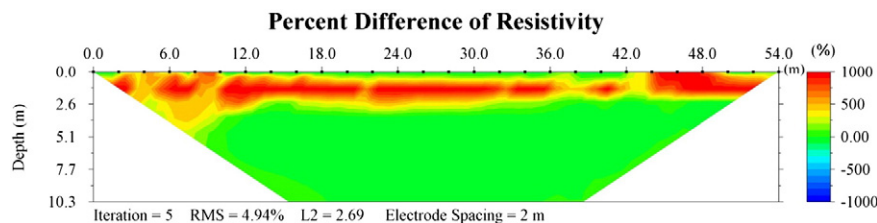


Fig. 10. ERT-2 results of the percent difference of resistivity between pre-remediation and post-remediation. Shallow resistivity increased by more than 10-fold. The increase in the resistivity represents the scope and depth of the excavation.

**Table 1**  
Statistics of sludge dumpsite FDEM data.

Sludge dumpsite			
	Date point	Average conductivity	Average in-phase
Pre-remediation	60	130.877 mS/m	9.587 ppt
Post-remediation	278	43.957 mS/m	2.909 ppt

Note: Data points analyzed coordinate on aerial photograph at (60, 140), (60, 130), (125, 145), and (125, 155).

integrity of the UST structure boundaries. Therefore, FDEM was chosen to complement and work with ERT after the GPR investigation. Testing was performed on the southwest side, known as low-contaminated potential, and in the north, known as high-contaminated potential where the sludge had rested. The results shown in Fig. 6A indicated that the surface conductivity was higher than 100 mS/m in areas where the sludge was found. In contrast, the surface conductivity was lower than 60 mS/m in areas without sludge. The material of the tank structure was reinforced concrete. FDEM is sensitive to metal. Therefore, values of high conductivity in the results determined the area and the integrity of the USTs. In other words, if the distribution range of the high conductivity was similar to the area where the USTs were located, the USTs could be presumed to be in a functional condition at the site; however, if the range of high conductivity mismatched with the range of the USTs or was greater than the range of USTs, this would indicate that the tanks were likely damaged. The results obtained from overlapping the conductivity contour map and the aerial photographs taken in 1990s revealed two high conductivity anomalies that were in two different sized rectangles and virtually identical to the area of USTs (Fig. 6B). As the two high anomalies clearly depicted the shape of the two different sized rectangles, FDEM self-confirmed its superiority in identifying the existence of USTs and revealing the exactness that the sludge was securely limited within the USTs. The UST excavation, shown in Fig. 7, indicated no red sludge between the two USTs, which meant there was no obvious contamination, and for this reason, the conductivity was rather low. Fig. 7 also indicated the position of the concrete partitioning. The partition structure not only caused the high resistivity showed at 27 m in ERT-1 pre-remediation investigation but also caused the discontinued high resistivity signals in ERT-1 post-remediation profile. In fact, the high conductivity detected by FDEM was the integrated signal reflected by subsurface materials, which could not be related to the sludge or the tanks. However, the ERT results showed signals of low resistivity (sludge) and high resistivity (UST) in the vertical resistivity distribution, and the sampling also suggested red sludge with a thickness of 1.2 m. Therefore, integrating the methods of ERT, FDEM and sampling, geophysical techniques can indeed achieve the main purpose of the site investigation, and assist remediation teams solving problems.

A post-remediation FDEM investigation was performed throughout the site (Fig. 8A), except in a small part in the southwest and the southeast areas in which there were newly planted artifacts that occupied the surface. The results showed that the surface area in the north, where the sludge piled, the conductivity decreased, with no apparent high electrical conductivity, reflecting that the shallow heavy-metal sludge had been replaced. In the southeast, the UST area, the conductivity declined slightly. Because the UST bottom structures still remained, the FDEM

**Table 2**  
Statistics of UST FDEM data.

UST area			
	Date point	Average conductivity	Average in-phase
Pre-remediation	2638	86.598 mS/m	12.780 ppt
Post-remediation	2350	81.807 mS/m	10.381 ppt

Note: Data points analyzed coordinate on aerial photographs at (150, 45), (140, 100), (250, 80), and (240, 135).

still measured the reaction of the reinforced structure. Thus, the conductivity measured was still highly biased. Overlapping the FDEM contour maps and the 1990s aerial photo (Fig. 8B) showed the pattern of the UST bottom structure in the southeast. In the north, the conductivity was lower than 60 mS/m, which was the reaction of the clean and contamination-free soil. This result also indirectly validated that the remediation work had been completed.

## 5. Discussion

### 5.1. GPR

Pre-remediation GPR probe failed to detect the bottom of the UST structure because the conductivity of the heavy-metal sludge was excessively high, severely attenuating the GPR signals. The attenuation of a radar wave ( $\alpha$ ) is approximately given by the following formula:

$$\alpha \approx 1690 \frac{\sigma}{\sqrt{K}} \quad (1)$$

where  $\sigma$  is the conductivity and  $K$  is the dielectric constant. This indicates that as the conductivity of a material increases, the radar wave attenuation grows. This attenuation becomes quicker and more distinct when the electromagnetic frequencies exceed 100 MHz (Davies and Annan, 1989), which was reason why the pre-remediation GPR did not realize the expected results. However, once the heavy-metal sludge was excavated and replaced with clean soil, the GPR could survey the signals from the tank bottom. Therefore, the post-remediation GPR indirectly verified the accomplishment of the remediation and can confirm the depth of excavation. GPR-2 profile was the post-remediation result of the southwest side (Fig. 9), in which 0.5 m was unearthed and backfilled. Fig. 9 showed an obvious interface at 10 ns. The continuous and smooth signals illustrated the interface and indicated the fact that even though it was not high-contamination-potential, the topsoil had been replaced by clean silt for 0.5 m depth. Compared with the signals below 10 ns, the original geological materials were rather weak. The weak resistivity signals were due to the background conductivity that was as high as ERT-2 disclosed. Although GPR-2 also showed signal attenuation, compared with pre-remediation GPR-1, the signal attenuation caused by the sludge was more severe.

### 5.2. ERT

The ERT-2 survey line in the sludge-filled area was controlled at nearly the same position for pre- and post-remediation investigations. The material property change could be understood from the percent difference of resistivity between pre- and post-remediation. Fig. 10 illustrated that the resistivity of the strata shallower than 2.5 m increased by 10 times more while elsewhere remained virtually the same, indicating that the material properties of the strata that were shallower than 2.5 m changed. The results demonstrated that the remediation team excavated the sludge area for more than 2.5 m deep.

### 5.3. FDEM

Both pre- and post-remediation FDEM surveyed in the north where the sludge dumpsite and the UST area had located. The statistical results were shown in Tables 1 and 2 with the coordinates on aerial photographs. The statistical results, shown in Table 1, illustrated that at the sludge dumpsite, the average post-remediation conductivity of 278 data points decreased to 43.957 mS/m; the in-phase signal decreased to 2.909 ppt, suggesting that the surface materials changed, and also verifies the complement of the remediation work. The statistical results, shown in Table 2, demonstrated that at the location of the UST, the average pre-remediation conductivity of 2638 data points was 86.598 mS/m,

with an in-phase signal of 12.780 ppt. Compared with the average pre-remediation conductivity in Table 1, the pre-remediation conductivity in Table 2 was lower. The reason for such numbers was because of the statistics, shown in Table 2, including the data from the contamination-free area between the USTs.

In fact, the highest conductivity was obtained in pre-remediation UST investigation, with no large difference from the post-remediation UST average conductivity (Table 2). The average post-remediation conductivity and in-phase signal were still high, and this was due to the reinforced concrete structure of UST bottom that remained. In FDEM surveys, if there is high conductivity material, such as metal, a great phase lag can cause negative-conductivity. Such an occurrence occurred in both pre- and post-remediation FDEM surveys; however, the negative values were less than 0.5% of the total data numbers and only occurred in UST area. When producing the conductivity contour maps and determining the overall average conductivity, the negative values were excluded.

FDEM collects data in grid arrangements that record a reading every 1 m to 2 m to create smooth contour maps and decrease misleading graphics (Paton, 2002). When the conductivity of the underground target object is similar to the background conductivity, this arrangement is necessary. Only if an accurate geodetic survey is conducted can an equidistant grid be applied. However, not all sites are smooth and even, which eases measurement and positioning, and time may be insufficient to preprocess measurements at every site and for every case. Time is a vital factor that determines the investigation method. In this study, FDEM collected data continuously; therefore, the amount of data was sufficient. The GPS coordinates of each measurement point were recorded simultaneously. In a pilot test, a difference of at least 40 mS/m was verified between the background conductivity and the probe targets. Therefore, by overlapping the contour map onto aerial photograph (Fig. 6B), the shapes of the USTs were the same as they had previously been, suggesting that the USTs remained. In fact, the UST distribution can be seen by simply overlapping the collected raw data onto aerial photograph (Fig. 6A). The operating time can be greatly reduced by omitting precise grid measurements and contour map drawing. In this case, for instance, all of the FDEM and ERT measurements were completed within one working day (12 h) and the figures of the results were immediately created, indicating that the UST remained intact at the site. Such a simplified procedure can be applied in time-pressing investigations; for example, assisting in disaster search and rescue. However, the precondition is that the distinct difference between the background conductivity and the abnormal conductivity is verified.

## 6. Conclusion

In this study, multiple geophysical prospecting techniques swiftly, efficiently and effectively solved the remediation issues and facilitated the subsequent remediation method design and budget estimation. Although GPR failed to meet the expectation in the pre-remediation investigation, ERT and FDEM accomplished the primary objectives of the UST investigation. Instead of negating the probing capabilities of GPR, the results indicated that each prospecting technique has its own advantages and limitations, differing in the strength of the signal reactions produced when the material properties change. Each geophysical prospecting method has its application under various environmental conditions. Multiple techniques combined can provide explanations from different views to complement each other. This is the current trend of applying geophysical techniques.

In comparison of the pre- and post-remediation investigations, the results can verify the accomplishment of the remediation. In pre-remediation investigations, FDEM can define the contaminated range or the distribution of the buried objects and GPR and ERT can determine the depth of the distribution of the pollution or the buried objects. Therefore, associated with sample analysis, they can clarify complex environments. In post-remediation investigations, the same process can

be employed to compare the differences between pre-remediation and post-remediation and to confirm and evaluate the remediation effectiveness. Effectively employing geophysical exploration techniques to investigate contaminated sites and evaluate remediation outcomes is beneficial in terms of time, cost, and effectiveness. In short, geophysical prospecting technology applications have extended from pre-remediation investigation to post-remediation assessment.

## Acknowledgment

We would like to thank Soil and Groundwater Pollution Remediation Fund Management Board for the support of this study. This study was funded under grant EPA-102-GA13-03-A258 of the Environmental Protection Administration, Executive Yuan, R. O. C. Many thanks go to the reviewers of this manuscript as well as the editors for their insightful and constructive comments for improving previous drafts of this paper.

## References

- Al-Nuaimy, W., Huang, Y., Nakhkash, M., Fang, M.T.C., Nguyen, V.T., Eriksen, A., 2000. Automatic detection of buried utilities and solid objects with GPR using neural networks and pattern recognition. *J. Appl. Geophys.* 43, 157–165.
- Annan, A.P., 2002. GPR—history, trends, and future developments. *Subsurf. Sens. Technol. Appl.* 3 (4), 253–270.
- Annan, A.P., Davis, J.L., 1976. Impulse radar sounding in permafrost. *Radio Sci.* 11 (4), 383–394.
- Annan, P., Bauman, P., Greenhouse, J.P., Redman, J.D., 1991. *Geophysics and DNAPLs*. *Groundw. Manag.* 5, 963–977.
- Atekwana, E.A., Atekwana, E.A., 2010. Geophysical signatures of microbial activity at hydrocarbon contaminated sites: a review. *Surv. Geophys.* 31, 247–283.
- Atekwana, E.A., Sauck, W.A., Werkema Jr., D.D., 2000. Investigations of geoelectrical signatures at a hydrocarbon contaminated site. *J. Appl. Geophys.* 44, 167–180.
- Ayolabi, E.A., Folorunso, A.F., Idem, S.S., 2013. Application of electrical resistivity tomography in mapping subsurface hydrocarbon contamination. *Earth Sci. Res.* 2 (1), 93–104.
- Barker, R.D., 1981. The offset system of electrical resistivity sounding and its use with a multicore cable. *Geophys. Prospect.* 29, 128–143.
- Barker, R.D., 1991. Depth of investigation of collinear symmetrical four-electrode arrays. *Geophysics* 54, 1031–1037.
- Barker, R.D., 1992. A simple algorithm for electrical imaging of the subsurface. *First Break* 10, 53–62.
- Batayneh, A.T., 2005. 2D electrical imaging of an LNAPL contamination, Al Amiriyya fuel station, Jordan. *J. Appl. Sci.* 5 (1), 52–59.
- Batmunkh, D., Tosun, S., Gundogdu, B., Candansayar, M.E., Ulugergerli, E.U., 2004. HLEM and magnetic surveys: examples from the Orkhun valley, Mongolia. *Archaeol. Prospect.* 11, 133–144.
- Beauprêtre, S., Garambois, S., Manighetti, I., Malavieille, J., S'en'echal, G., Chatton, M., Davies, T., Larroque, C., Rousset, D., Cotte, N., Romano, C., 2012. Finding the buried record of past earthquakes with GPR-based palaeoseismology: a case study on the Hope fault, New Zealand. *Geophys. J. Int.* 189, 73–100.
- Bowling, J.C., Harry, D.L., Rodriguez, A.B., Zheng, C., 2007. Integrated geophysical and geological investigation of a heterogeneous fluvial aquifer in Columbus Mississippi. *J. Appl. Geophys.* 62, 58–73.
- Cassidy, N.J., 2007. Evaluating LNAPL contamination using GPR signal attenuation analysis and dielectric property measurements: practical implications for hydrological studies. *J. Contam. Hydrol.* 94, 49–75.
- Chang, P.Y., Chen, C.C., Chang, S.K., Wang, T.B., Wang, C.Y., Hsu, S.K., 2012. An investigation into the debris flow induced by typhoon Morakot in the SiaoLin Area, Southern Taiwan, using the electrical resistivity imaging method. *Geophys. J. Int.* 188 (3), 1012–1024.
- Conyers, L.B., Ernenwein, E.G., Grealy, M., Lowe, K.M., 2008. Electromagnetic conductivity mapping for site prediction in meandering river floodplains. *Archaeol. Prospect.* 15 (2), 81–91.
- Dahlin, T., Zhou, B., 2004. A numerical comparison of 2D resistivity imaging with 10 electrode arrays. *Geophys. Prospect.* 52, 379–398.
- Dahlin, T., Bernstons, C., Gundogdu, B., Loke, M.H., 2002. A 3-D resistivity investigation of a contaminated site at Lemacken, Sweden. *Geophysics* 67 (6), 1692–1700.
- Davis, L., Annan, A.P., 1989. Ground-penetrating radar for high-resolution mapping of soil and rock stratigraphy. *Geophys. Prospect.* 37, 531–551.
- Godio, A., Naldi, M., 2003. Two-dimensional electrical imaging for detection of hydrocarbon contaminants. *Near Surf. Geophys.* 1, 131–137.
- Goes, B.J.M., Meekes, J.A.C., 2004. An effective electrode configuration for the detection of DNAPLs with electrical resistivity tomography. *J. Environ. Eng. Geophys.* 9 (3), 127–141.
- Greenhouse, J., Brewster, M., Schneider, G., Redman, D., Annan, P., Olhoeft, G., Lucius, J., Sander, K., Mazzella, A., 1993. *Geophysics and solvents: the Borden experiment*. *Lead. Edge* 12, 261–267.
- Griffiths, D.H., Barker, R.D., 1993. Two-dimensional resistivity imaging and modelling in areas of complex geology. *J. Appl. Geophys.* 29, 211–226.
- Griffiths, D.H., Turnbull, J., 1985. A multi-electrode array for resistivity surveying. *First Break* 3 (7), 16–20.

- Griffiths, D.H., Turnbull, J., Olayinka, A.I., 1990. Two-dimensional resistivity mapping with a computer-controlled array. *First Break* 8, 121–129.
- Guérin, R., Munoz, M.L., Aran, C., Laperrelle, C., Hidra, M., Drouart, E., Grellier, S., 2004. Leachate recirculation: moisture content assessment by means of a geophysical technique. *Waste Manag.* 24 (8), 785–794.
- Halihan, T., Paxton, S., Graham, I., Fenstemaker, T., Riley, M., 2005. Post-remediation evaluation of LNAPL site using electrical resistivity imaging. *J. Environ. Monit.* 7, 283–287.
- Hermozilha, H., Grangeia, C., Matias, M.S., 2010. An integrated 3D constant offset GPR and resistivity survey on a sealed landfill – Ilhavo, NW Portugal. *J. Appl. Geophys.* 70, 58–71.
- Holman, I.P., Hiscock, K.M., 1998. Land drainage and saline intrusion in the coastal marshes of northeast Norfolk. *Q. J. Eng. Geol. Hydrogeol.* 31 (1), 47–62.
- Lago, A.L., Elis, V.R., Borges, W.R., Penner, G.C., 2009. Geophysical investigation using resistivity and GPR methods: a case study of a lubricant oil waste disposal area in the city of Ribeirão Preto, São Paulo, Brazil. *Environ. Geol.* 58, 407–417.
- Loke, M.H., 1994. The inversion of two-dimensional resistivity data. Unpubl. PhD thesis, Un. Of Birmingham.
- Loke, M.H., Wilkinson, P., Chambers, J., 2010a. Fast computation of optimized electrode arrays for 2D resistivity surveys. *Comput. Geosci.* 36, 1414–1426.
- Loke, M.H., Wilkinson, P., Chambers, J., 2010b. Parallel computation of optimized arrays for 2-D electrical imaging. *Geophys. J. Int.* 183, 1202–1315.
- Loke, M.H., Chambers, J.E., Rucker, D.F., Kuras, O., Wilkinson, P.B., 2013. Recent developments in the direct-current geoelectrical imaging method. *J. Appl. Geophys.* 95, 135–156.
- Lopes de Castro, D., Branco, R.M.G.C., 2003. 4-D ground penetrating radar monitoring of a hydrocarbon leakage site in Fortaleza (Brazil) during its remediation process: a case history. *J. Appl. Geophys.* 54, 127–144.
- Martínez-Pagán, P., Cano, A.F., Silva, G.R., Olivares, A.B., 2010. 2-D electrical resistivity imaging to assess slurry pond subsoil pollution in the southeastern region of Murcia, Spain. *J. Environ. Eng. Geophys.* 15 (1), 29–47.
- McNeill, J.D., 1980. Electromagnetic Terrain Conductivity Measurement at Low Induction Numbers. Geonics, Technical Note TN-6.
- McNeill, J.D., 1990. Use of electromagnetic methods for groundwater studies. In: Ward, S.N. (Ed.), *Geotechnical and Environmental Geophysics: I. Review and Tutorial*. Society of Exploration Geophysicists, Tulsa, OK, pp. 191–218.
- Mussett, A.E., Khan, M.A., 2000. *Looking into the Earth: An Introduction to Geological Geophysics*. Cambridge University Press.
- Nobes, D.C., 1999. How important is the orientation of a horizontal loop EM system? Examples from a leachate plume and a fault zone. *J. Environ. Eng. Geophys.* 4 (2), 81–85.
- Nobes, D.C., Armstrong, M.J., Close, M.E., 2000. Delineation of a landfill leachate plume and flow channels in coastal sands near Christchurch, New Zealand, using a shallow electromagnetic survey method. *Hydrogeol. J.* 8 (3), 328–336.
- Ny'ari, Z., Kanh, A.I., 2007. Imaging of buried 3D objects by using electrical profiling methods with GPR and 3D geoelectrical measurements. *J. Geophys. Eng.* 4, 83–93.
- Orlando, L., 2013. GPR to constrain ERT data inversion in cavity searching: theoretical and practical applications in archeology. *J. Appl. Geophys.* 89, 35–47.
- Paton, D.G., 2002. Influence of travel speed, data collection rate and pattern on EM contours (You can never have too much data, right?). 15th EEGS Symposium on the Application of Geophysics to Engineering and Environmental Problems (Las Vegas, NV).
- Pettersson, J.K., Nobes, D.C., 2003. Environmental geophysics at Scott Base: ground penetrating radar and electromagnetic induction as tools for mapping contaminated ground at Antarctic research bases. *Cold Reg. Sci. Technol.* 37, 187–195.
- Porsani, J.L., Slob, E., Lima, R.S., Leite, D.N., 2010. Comparing detection and location performance of perpendicular and parallel broadside GPR antenna orientations. *J. Appl. Geophys.* 70, 1–8.
- Pringle, J.K., Jervis, J.R., Hansen, J.D., Jones, G.M., Cassidy, N.J., Cassella, J.P., 2012. Geophysical monitoring of simulated clandestine graves using electrical and ground-penetrating radar methods: 0–3 years after burial. *J. Forensic Sci.* 57 (6), 1467–1486.
- Soupios, P., Papadopoulos, N., Papadopoulos, I., Kouli, M., Vallianatos, F., Sarris, A., Manios, T., 2007. Application of integrated methods in mapping waste disposal areas. *Environ. Geol.* 53, 661–675.
- Tohge, M., Karube, F., Kobayashi, M., Tanaka, A., Ishii, K., 1998. The use of ground penetrating radar to map an ancient village buried by volcanic eruptions. *J. Appl. Geophys.* 40, 49–58.
- Tong, L.T., Lee, K.H., Yeh, C.K., Hwang, Y.T., Chien, J.M., 2013. Geophysical study of the Peinan Archaeological Site, Taiwan. *J. Appl. Geophys.* 89, 1–10.
- Vaudelet, P., Schmutz, M., Pessel, M., Franceschi, M., Guérin, R., Atteia, O., Blondel, A., Ngomseu, C., Galaup, S., Rejiba, F., Bégassat, P., 2011. Mapping of contaminant plumes with geoelectrical methods. A case study in urban context. *J. Appl. Geophys.* 75, 738–751.
- Wightman, W., Jalinoos, F., Sirls, P., Hanna, K., 2004. Application of Geophysical Methods to Highway Related Problems (No. FHWA-IF-04-021).
- Yang, X., 1999. Stochastic Inversion of 3-D ERT Data. Univ. Arizona (PhD thesis).
- Yu, C.Y., Hsiao, K.P., Liu, H.C., 2009. Results of geological survey and remains search in Hsiao-Lin and Hsin-Kai village after typhoon Morakot September 21 2009, National Science and Technology Center for Disaster Reduction Newsletter 50 (Retrieved October 12, 2009, from <http://www.ncdr.nat.gov.tw> (in Chinese)).
- Zhou, B., Dahlin, T., 2003. Properties and effects of measurement errors on 2D resistivity imaging. *Near surf. Geophys.* 1, 105–117.
- Zogala, B., Robak, M., Dubiel, R., Zuberek, W.M., Steininger, M., Wzienter, K., 2009. Geoelectrical methods for detection of oil contaminations in soil and bioremediation process monitoring. 22nd EEGS Symposium on the Application of Geophysics to Engineering and Environmental Problems, pp. 348–362 (Fort Worth, Texas).